

Storm surge and tidal interaction in the Tjeldsund channel, northern Norway

Birgit Kjoss Lyngre · Karina Hjelmervik · Bjørn Gjevik

Received: 19 September 2012 / Accepted: 7 May 2013
© Springer-Verlag Berlin Heidelberg 2013

Abstract The aim of this study is to investigate tide–surge interaction in narrow channels with complex and relatively shallow topography. A high-resolution depth-integrated tidal and storm surge model has been implemented for the Tjeldsund channel which is an important sailing lane in northern Norway. A horizontal grid resolution down to 50 m is applied in order to represent the complex bottom topography and the formation of jets and small-scale eddies. Two typically storm surge events in December 2004 have been examined in detail. The tide–surge interaction is found to influence the generation of higher harmonics and the formation of eddies in the current field. In some cases, the magnitude of storm surge currents may reach the same magnitude as the tidal currents enhancing the formation of jets and eddies.

Keywords Tide–surge interaction · Storm surge · Tidal model · Northern Norway

Responsible Editor: Birgit Andrea Klein

B. K. Lyngre (✉) · B. Gjevik
Department of Mathematics, University of Oslo,
P.O. Box 1053, Blindern, 0316 Oslo, Norway
e-mail: birgit.lyngre@rolls-royce.com

B. Gjevik
e-mail: bjornng@math.uio.no

K. Hjelmervik
Department of Maritime Technology and Innovation,
Vestfold University College,
P.O. Box 2243, 3103 Tønsberg, Norway
e-mail: karina.hjelmervik@hive.no

1 Introduction

The non-linear interaction between tides and storm surges has been studied extensively by e.g. Prandle and Wolf (1978), Johns et al. (1985), Tang et al. (1996), Bobanovic et al. (2006), Horsburgh and Wilson (2007), Jones and Davies (2007, 2008), and references therein. The focus has mostly been on how the interaction affects the elevation of the surge and the timing of high water relative to the phase of the tide. The non-linear quadratic bottom friction, used in most shallow water models, is found to play a crucial role for the tide–surge interaction, but the coupling between the surge and the tide through the non-linear momentum terms is also important. The latter mechanism is particularly important for the non-linear modification of the current field by generation of higher harmonics and short periodic current oscillations by shear flow instabilities. In shallow water regions, the tide–surge interaction may both influence the surge and modify the tide at the time of the surge (Jones and Davies 2008).

In the present study, we study the tide–surge interaction in the narrow and relatively shallow Tjeldsund channel which connects two large and deeper fjord systems; the Vestfjord and the Vågsfjord in the Lofoten area in northern Norway (Figs. 1 and 2). The channel is an important sailing lane for coastal traffic, also including large vessels. The tidal range is about 4 m at Narvik at the head of the Vestfjord and 3 m at Harstad in the Vågsfjord. The tides in this area have previously been modelled with a regional model with 500 m horizontal grid resolution (Gjevik et al. 1997; Moe et al. 2002). More recently, Hjelmervik et al. (2005, 2009) used a high-resolution model with horizontal grid resolution down to 25 m to simulate the tidal flow in the Tjeldsund channel. In the latter paper, some aspects of the tide and surge interaction were also discussed.

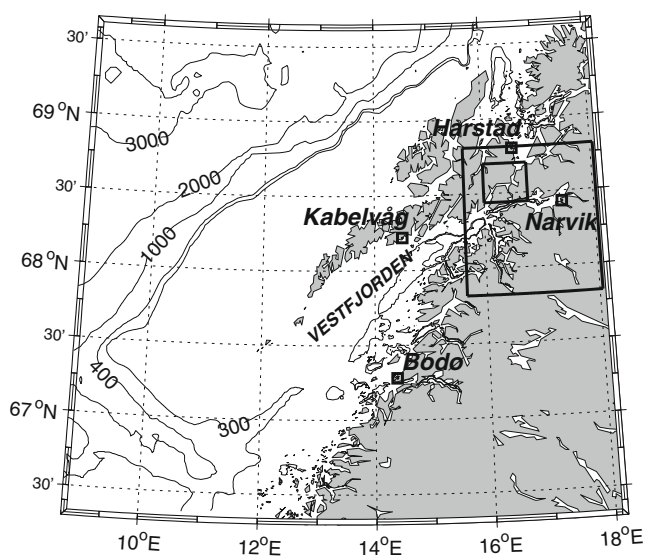


Fig. 1 Location of the two model domains (rectangles) on the northern coast of Norway. Enlargement of the smaller domain is shown in Fig. 2. Depth contours in metres

During a storm situation, with low atmospheric pressure and strong south-westerly wind, the sea level in the inner part of the Vestfjord often rises up to 1 m due to the atmospheric forcing. The large-scale external surge in the fjords can in such situations lead to sea level differences up to 1 m between the ends of the Tjeldsund channel. This can introduce a current through the channel of the order 1 m s^{-1} , which is of comparable strength to the tidal current. The current associated with strong storm surge events is mainly

driven by external surge in the deep fjords north and south of the channel. The local wind stress on the water masses within the channel contributes less to the current due to the sheltering effect by the high and irregular mountains in the area.

The surge current may intensify or reduce the tidal current depending on the phase of the tide relative to the timing of the peak surge-driven current. In narrow and shallow parts of the channel, the current can also be strong enough to produce non-linear interaction between the surge and the tide with the generation of higher harmonics, flow separation with eddies at bends in the channel, and short periodic current oscillation due to shear flow instability. In contrast to the situation in most estuaries, the maximum tidal current in the Tjeldsund channel occurs nearly at the time of high and low water, respectively. To our knowledge, this particular tide–surge interaction problem in a narrow channel has not been reported previously. The focus will be on well-mixed conditions which usually occur during autumn and winter. Hence, we will use the depth-integrated shallow water equations which have been applied extensively for modelling tides and storm surges in shelf and coastal areas (Davies et al. 1997a, b, and references therein).

The challenges with numerical modelling of the tidal and storm surge current in the Lofoten area are many. First of all, the complex bottom topography and coastline require a very fine spatial grid resolution. Secondly, in order to capture the formation of narrow jets and small-scale eddies, it is essential that the numerical scheme maintains the correct balance between advection and dissipation terms in the equations of motion.

Fig. 2 The area of interest is the Tjeldsund channel with the Ramsund branch to the right. Bottom topography is shown by colour shading with depth in metres on the scale. Depths are related to mean sea level. Location of the stations with current measurements are marked St1–St3 and SK



In narrow channels and sailing lanes with busy traffic as in Tjeldsund, the current represents a considerable safety hazard. Currents of 1 m s^{-1} may introduce forces on large ships of the same order of magnitude as gale force winds. This may make it difficult to manoeuvre large ships in the channel, with the risk of being carried off the recommended sailing lane. Wave–current interaction may also introduce additional complications for safe sailing (Hjelmervik and Trulsen 2009). If the current field can be predicted with a reasonable accuracy, this may improve the safety of sailing and reduce the risk for ship collisions and groundings. Accurate predictions of currents may also prove valuable during cleanup operations after oil spill disasters and search, rescue, and surveillance operations during ship accidents.

Recently, it has been demonstrated how predicted high-resolution tidal current fields can be displayed in real time on modern electronic navigational charts, and thereby become a useful tool for navigators (Gjevik et al. 2006).

2 Numerical model

2.1 Model equations

The non-linear depth-integrated shallow water equations in a Cartesian coordinate system (x, y, z) with the x - and y -axis horizontal in the level of the undisturbed surface are given by:

$$\frac{\partial \eta}{\partial t} = -\frac{\partial U}{\partial x} - \frac{\partial V}{\partial y} \tag{1}$$

$$\frac{\partial U}{\partial t} + \frac{\partial}{\partial x} \left(\frac{U^2}{H} \right) + \frac{\partial}{\partial y} \left(\frac{UV}{H} \right) - fV = -gH \frac{\partial \eta}{\partial x} + F^x + A^x \tag{2}$$

$$\frac{\partial V}{\partial t} + \frac{\partial}{\partial x} \left(\frac{UV}{H} \right) + \frac{\partial}{\partial y} \left(\frac{V^2}{H} \right) + fU = -gH \frac{\partial \eta}{\partial y} + F^y + A^y \tag{3}$$

where t is the time, (U, V) are the components of volume flux vector per unit length in the horizontal plane, η the vertical displacement of the sea surface from the mean sea level, $H = H_0 + \eta$ the total depth, H_0 the mean depth, g the acceleration of gravity, and f the Corioli parameter. The bottom friction terms, F^x and F^y , are given by:

$$F^{x,y} = -c_D \frac{(U, V)}{H} \frac{\sqrt{U^2 + V^2}}{H}, \tag{4}$$

where c_D is the drag coefficient of the quadratic bottom shear stress. The horizontal eddy viscosity terms, A^x and A^y , are parameterized by a simple large eddy simulation model:

$$A^{x,y} = \nu \frac{\partial^2}{\partial x^2} (U, V) + \nu \frac{\partial^2}{\partial y^2} (U, V) \tag{5}$$

or

$$A^{x,y} = \frac{\partial}{\partial x} \left(\nu \frac{\partial}{\partial x} (U, V) \right) + \frac{\partial}{\partial y} \left(\nu \frac{\partial}{\partial y} (U, V) \right), \tag{6}$$

where ν is the eddy viscosity coefficient of the horizontal shear stress. Equation 6 is applied for all simulations except the tidal simulations in Section 3 where Eq. 5 is applied. The eddy viscosity coefficient is expressed according to Smagorinsky (1963), by:

$$\nu = ql^2 \left[\left(\frac{\partial \bar{u}}{\partial x} \right)^2 + \frac{1}{2} \left(\frac{\partial \bar{u}}{\partial y} + \frac{\partial \bar{v}}{\partial x} \right)^2 + \left(\frac{\partial \bar{v}}{\partial y} \right)^2 \right]^{\frac{1}{2}}, \tag{7}$$

where q is a constant, l is a length scale which is set equal to the grid size, and (\bar{u}, \bar{v}) denote the components of the depth mean current velocity defined to the first order by:

$$\bar{u} = \frac{U}{H}, \quad \bar{v} = \frac{V}{H}$$

With $q = 0.5$, a grid size of 100 m, and a current speed of the order 1 m s^{-1} , Eq. 7 leads to an eddy viscosity coefficient of the order $50 \text{ m}^2 \text{ s}^{-1}$.

The model equations 1–3 are discretized on a quadratic C-grid (Mesinger and Arakawa 1976) with a finite difference numerical scheme centred in space and forwarded in time. The advection terms are estimated with an extrapolation routine for the grid points near the coastal boundaries in order to avoid one-sided differences. Further details on how the numerical scheme is designed and its performance for this particular application can be found in Hjelmervik et al. (2005).

The CFL-stability criterion satisfied by the numerical time step, Δt , is:

$$\Delta t \leq \frac{\Delta x}{\sqrt{2gH_{\max}}}, \tag{8}$$

where H_{\max} is the maximum depth of the model domain.

2.2 Model setup and boundary conditions

The area of interest is the narrow and shallow parts of the Tjeldsund channel and the Ramsund branch shown in Fig. 2.

By using a relatively small domain, we are able to refine the resolution. In order to justify the use of a small domain, the numerical model was set up for the two rectangular domains shown in Fig. 1. Model simulations with a horizontal grid resolution $\Delta x = \Delta y$ ranging from 25 to 100 m have been performed, 25 and 50 m for the smaller domain, and 100 m for the larger domain. Comparisons between simulations for the two domains show only small deviations, and justify the use of the smaller domain for our purpose

(Hjelmervik et al. 2009). The results presented in this paper are from the smaller domain using a horizontal equidistant grid with resolution 50 m. The high-resolution bottom topography is based mainly on multibeam bathymetric data from Norwegian Hydrographic Service (NHS). Depths are related to mean sea level.

The area of interest (Fig. 2) has two open boundaries towards the Vestfjord on the southern end of the channel and one towards the Vågsfjord on the northern end of the channel. The south-westerly corner of the domain has coordinates $X = 541250$ and $Y = 7593800$ (given to WGS84-UTM zone 33) and the domain covers 39×27 km in the x, y directions, respectively. The coordinate axis (x, y) are orientated west-east and south-north, respectively.

As driving force, surface elevation is specified at the open boundaries. Simulations have been carried out with three different types of boundary forcing:

1. Surface elevation from tide only,
2. Surface elevation from storm surge, and
3. The total sea level (tide+storm surge).

The open boundaries are located in broad and relatively deep fjords where non-linear interactions are less important. The tide–surge interaction on the open boundaries are therefore neglected, and the storm surge boundary forcing is obtained simply by subtracting the predicted tide from the observed sea level signal. That a linear decomposition of the tide and the surge is possible in deep water was also anticipated by Jones and Davies (2008). Local wind stress has been neglected in our experiments. This conjecture is based on the assumption that the external sea level south and north of the Tjeldsund channel is the main driving force for the flow through the channel, and that the local wind stress in the channel is of minor importance.

Tidal predictions and constituents were obtained from sea level data from the permanent NHS recording stations at Narvik and Harstad located in the vicinity of the model area (Fig. 1). At the two southern open boundaries in Tjeldsund (A) and Ramsund (B) (see Fig. 2) we have extrapolated sea level data westward from Narvik. Amplitude is reduced with a factor 0.97 and 0.99, respectively, compared to the data from Narvik. At the northern boundary (C), we have extrapolated southward from Harstad, and the amplitude is increased with a factor 1.01 compared to the data from Harstad. The factors are based on the relation between sea level observations in the area of interest and the permanent tide gauges at Narvik and Harstad (NHS). In view of the small differences in phases between Narvik and Harstad and the respective open boundaries, no corrections have been made to the phases.

At the open boundaries, the flow relaxation scheme (Martinsen and Engedahl 1987) has been used to impose the

boundary conditions. Surface elevation is updated in every time step according to

$$\phi = (1 - \alpha)\phi_{\text{int}} + \alpha\phi_{\text{ext}}, \quad (9)$$

where ϕ_{int} contains the unrelaxed values computed by the model, and ϕ_{ext} is a specified external value. The relaxation parameter varies smoothly from 1 at the open boundary to 0 at the innermost cell of the boundary zone. The rationale behind this scheme is to soften the transition from an exterior solution to an interior solution by use of a grid zone where the two solutions dominate at each ends respectively. The width of the zone is taken to be ten grid cells.

All simulations started from rest (U, V and η equal to 0) with increasing boundary forcing in time according to a ramping function, $(1 - \exp(-\sigma t))$. A value of $\sigma = 4.6 \times 10^{-5} \text{ s}^{-1}$ has been used. This implies full driving effect of the boundary conditions after about 12 h.

Among the challenges for simulations with non-linear advection terms for this complicated coastline configuration and bathymetry is to obtain stable solutions by adjusting the horizontal eddy viscosity. In order to check the sensitivity of the solutions to different values of eddy diffusivity parameters, a series of separate simulations have been done for the semi-diurnal M_2 component. Based on the results of Hjelmervik et al. (2005), we have chosen $q = 0.5$ for grid size $\Delta x = 50$ m. The large value of $c_D = 0.0075$ is also in accordance with other high-resolution models as for example, Sutherland et al. (2005).

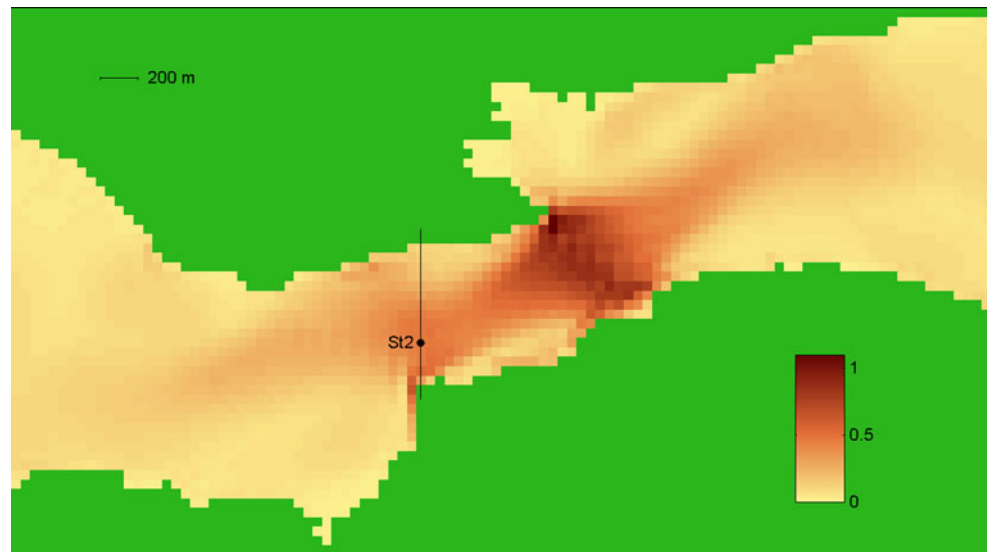
A 24 h spin up time is found to be sufficient to obtain an acceptable steady state. After 48 h, complete fields for current and elevation data are stored every hour. Data for surface elevation, current strength and direction from selected stations (grid nodes) were stored with 180 s sampling for later processing.

3 Tidal simulations

The area of interest (Fig. 2) is nested into larger models. Earlier tidal simulations have been carried out for the entire domain covered by the map in Fig. 1, with 500 m horizontal grid resolution (Moe et al. 2002). Results from these simulations have been used to obtain interpolated boundary conditions for the domain marked with the larger rectangle in Fig. 1 (Hjelmervik et al. 2009). And results from these simulations have been used to obtain interpolated boundary conditions for the area of interest marked with the smaller rectangle in Fig. 1.

The depth-integrated model has been run for the four major tidal constituents, i.e. the three major semi-diurnal components M_2, S_2, N_2 , and the major diurnal component K_1 , for the two rectangular domains marked in Fig. 1. The modelled current fields displayed the characteristic

Fig. 3 The tidal current level in the Ballstadstraum displayed by contour plot of the M_2 major current axis. Colour scale in m s^{-1} . The cross section for volume flux calculations and the station for current records are marked



features of the tidal current in the Tjeldsund and Ramsund channels. The three areas with the strongest currents are localised at Ballstad, Sandtorg, and Steinsland, see Fig. 2. The horizontal variation in the current field at Ballstad is shown in Fig. 3.

For a period from November 2004 to March 2005 current measurements were executed at two locations in the Tjeldsund channel, at Steinsland and Ballstad (St1 and St2, respectively, in Fig. 2). See Section 6 for more details on the field measurements. A detailed comparison between modelled and observed tidal parameters is given in Hjelmervik et al. (2009), also including current records from 1985 station SK (Fig. 2). Maximum current speed through various sections of the channel were found to occur around time of high and low water (Fig. 4), in agreement with observations.

Detailed plots of the current fields reveal a system of eddies which are controlled to a large extent by the bathymetry and the bottom friction. The effects of

the over-harmonic tidal components were also examined, mainly M_2 , M_4 , and M_6 , with periods 8.28, 6.21, and 4.14 h, respectively. While the sea level amplitude of the over-harmonics are small and less than 3% of the M_2 amplitude, the over-harmonics are much more pronounced in the simulated current data, i.e. 5–14% of the M_2 amplitude in the mean current in the cross sections at Ballstad, Sandtorg, and Steinsland. The amplitude of the over-harmonics varies considerably over relatively short distances, and are to a large extent associated with eddies, either topographically trapped or slowly propagating (Hjelmervik et al. 2009).

4 Storm surge events

In the period November 2004–April 2005, current sensors deployed in the Tjeldsund and Ramsund channels

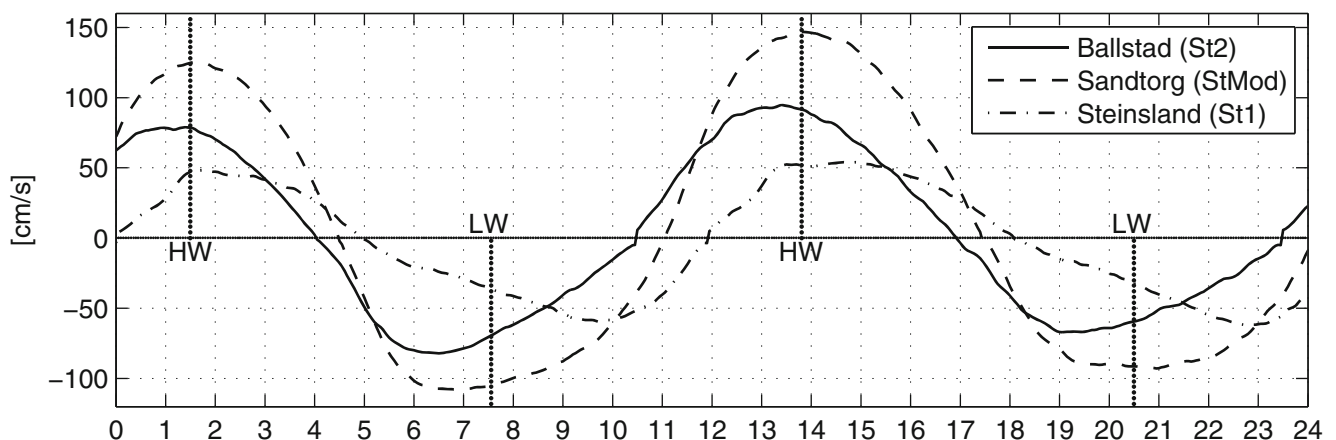
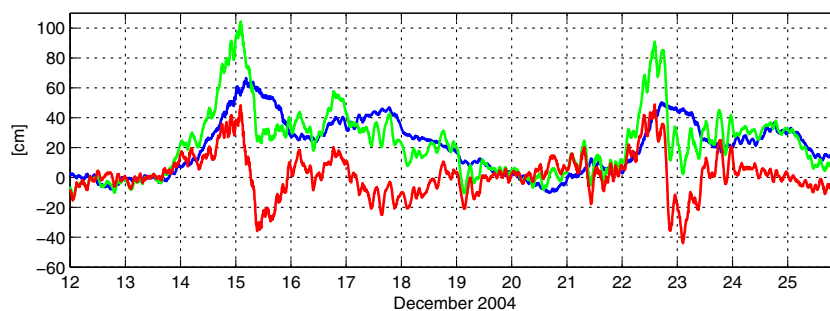


Fig. 4 Modelled tidal current speed relative to local high and low water on 15 December 2004 (24 h UT) at Ballstad (station St2), Sandtorg (StMod), and Steinsland (station St1) (Fig. 2). Positive value for north-east and negative for south-west

Fig. 5 Residual sea level (observed sea level minus predicted tide) from Narvik (green) and Harstad (blue) and residual difference (Narvik minus Harstad) (red) for the period 12–26 December 2004



captured several storm surge events. During the storm surge events, the surge sea level reached up to about 100 cm in Narvik at the southern entrance of the Tjeldsund channel, and up to 70 cm in Harstad at the northern entrance of the channel (NHS), which is comparable to mean high water. The highest measured surge level in the area of interest was measured to 135 cm in Narvik January 2006. In December 2004, the storm surges introduced additional sea level differences up to 50 cm between the southern and the northern entrances of the channel which modified the tidal current pattern. The residual sea level (observed sea level minus predicted tide) from Harstad in the north and Narvik in south are shown in Fig. 5 together with the residual sea level difference between Narvik and Harstad. Since both Narvik and Harstad are located in relatively deep fjords, the effect of non-linear interaction between the surge and the tide is believed to be negligible for these stations (see Section 2.2). We have examined in detail two cases which represent typical strong storm surge events in the area.

Case I, 12–16 December 2004: Surface weather map from 15 December 00:00 UT shows a 960-hPa deep depression with centre west of Lofoten, at N70°, E5° (Fig. 6). It caused strong south-westerly winds in the Vestfjord. The combined effect of wind and low air pressure induced a higher sea level in the Vestfjord and the inner extension called the Ofotfjord. The storm surge event occurred shortly after new moon 12 December, i.e. during a spring tide with stronger tidal currents. In Narvik, the storm surge reached its maximum (104 cm, predicted tide subtracted) at 02:10 UT on 15 December, shortly after the time of high tide at 01:30 UT. Residual sea level was high for about 10 h before maximum occurred. In Harstad, the storm surge reached maximum (67 cm) at 04:30 UT at ebbing tide. The difference in residual sea level between Narvik and Harstad was about 30–40 cm for about 10 h reaching a maximum 48 cm at 02:10 UT 15 December, with residual sea level higher in Narvik than in Harstad. At 06:30 UT 15 December, the residual sea level difference reversed, changing to minus 36 cm at 09:20 UT. The residual sea level difference stayed at about minus 25 cm for about 10 h.

Case II, 20–24 December 2004: The weather situation was similar to Case I and the surface weather maps from

23 December, 00:00 UT shows an unusual deep depression (935 hPa) with centre west of Lofoten at N73°, E5°. The south-westerly wind and low air pressure lead to high sea level in the Vestfjord. The storm surge event occurred shortly after half-moon 18 December and hence during neap tide. The storm surge reached maximum (91 cm) in Narvik 14:10 UT 22 December just before ebb at 15:00 UT and remained quite high for about 8 h. In Harstad, the storm surge reached its maximum (50 cm) at 17:10 UT about 4 h before high tide at 21:15 UT 22 December. Residual sea level stayed at the same level about one tidal period (12.5 h) during high and low tide. The difference in residual sea level between Narvik and Harstad attained its maximum (49 cm) at 14:10 UT 22 December (highest in Narvik) and the maximum reverse difference (44 cm) occurred at 02:30 UT 23 December.

5 Tide–surge interaction mechanism

In order to investigate the interaction between the tidal current and the additional current induced by the storm surge,

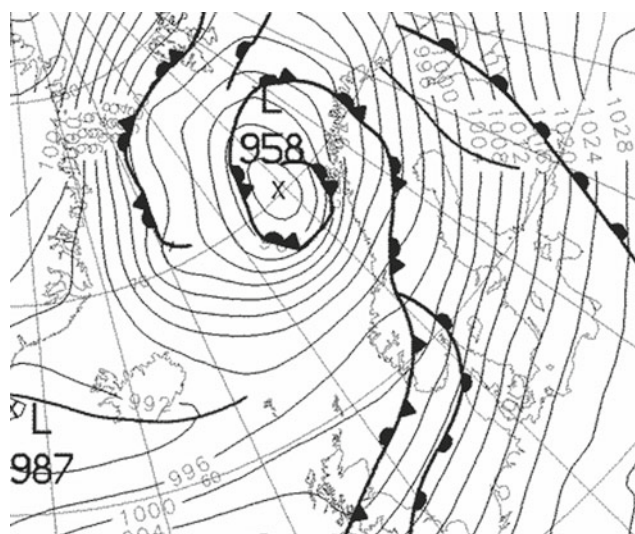


Fig. 6 Surface weather map from 15 Dec 2004 00:00 UT (From UK Met Office archive)

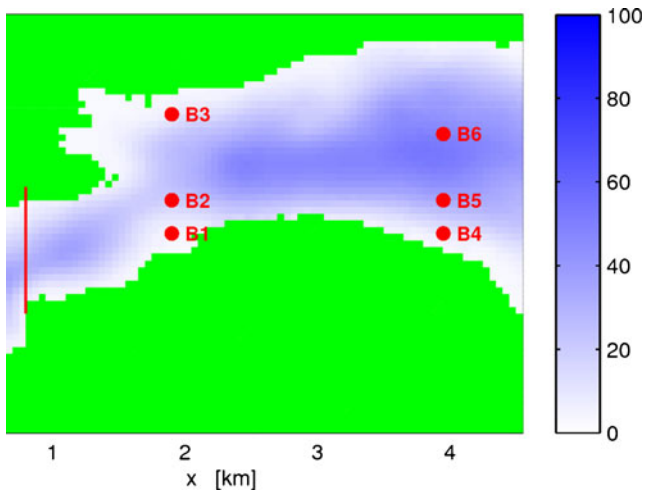


Fig. 7 Bathymetry of the Ballstadstraumen area with cross section for mean current flux calculations and the locations B1–B6 used for harmonic analyses. Colour bar for depth in metres

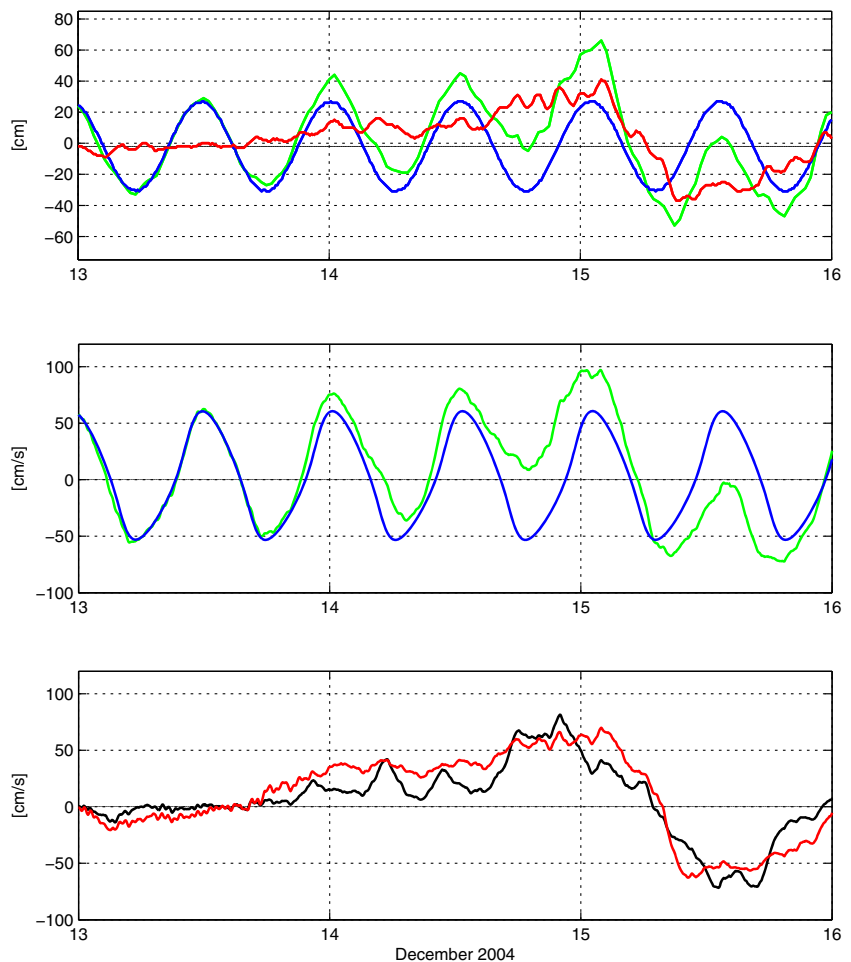
the model has been run for the area of interest (Fig. 1) for eight M_2 tidal periods (after a 24 h spin up) on a 50 m grid. Simulations have been carried out with three different types

of boundary forcing (see Section 2.2) for the two storm surge events in December 2004 described in Section 4.

For the simulations presented here, the tidal forcing is represented only by the major semi-diurnal tidal constituent M_2 . This was done in order to be able to study the interaction mechanism more closely by harmonic analyses of the relatively short simulated current time series with length comparable to the duration of the surge. A similar approach, studying only the effect of M_2 , was advocated by Jones and Davies (2008).

We concentrate the investigation of the interaction mechanism for an area in the shallow Ballstadstraumen, see Fig. 2, where the tidal simulations show strong current, flow separation and topographically trapped eddies. The mean current through the cross section, shown in Figs. 3 and 7, has been used as an integrated measure of the current conditions in the channel. In the following discussion, we use the term tidal current for the current obtained by only M_2 boundary forcing, total current for the combined effect of storm surge and M_2 -tide, and storm surge current for the current obtained by only storm surge forcing at the boundaries.

Fig. 8 Case I: 13–15 December 2004. *Upper panel:* Sea level difference between Narvik and Harstad, predicted M_2 tide (blue), storm surge (red), and tide+surge (green). *Middle panel:* Modelled mean current through the cross section at the Ballstadstraumen. Tidal M_2 current only (blue), tide+storm surge current (green). *Lower panel:* Modelled mean storm surge current through the cross section at the Ballstadstraumen (red), and the difference between the modelled tide+storm surge current and modelled tidal M_2 current (black), which is the difference between the green and the blue line in middle panel. Positive values indicate eastward direction



5.1 Effects of the storm surge events

The storm surge events introduce a difference between the sea level at the northern and southern entrance of the channel of up to 0.7 m. This intensifies or reduces the tidal current according to the time of the surge relative to the phase of the tide. The total volume fluxes through cross sections of the channel are found to be nearly proportional to the sea level difference between the northern and southern entrances. This is clearly seen by comparing the storm surge difference between the northern and southern entrance and the modelled storm surge current in the cross section at Ballstad (upper and lower panels of Figs. 8 and 9). We note that the storm surge current in both cases is persistent in the same direction for up to 24 h, i.e. longer than the semi-diurnal tidal oscillation. The total current is at its strongest when maximum tidal current and maximum storm surge current are in phase and contributes in the same direction. That is when maximum difference in tidal elevation between the northern and southern entrances coincide with the corresponding maximum difference in the storm surge. This situation occurred during Case I early on 15

December (Fig. 8) when the eastward storm surge current and the eastward tidal current reached maximum at about the same time. Figure 10 shows the tidal current in the Ballstadstraum at 02:00 UT 15 December while Fig. 11, from the same site, shows how the storm surge and the tidal current add up to an intensified current. This also affects the topographically trapped eddies respectively on the northern and southern sides of the channel. A similar situation occurred during Case II early on 23 December when the westward storm surge current and the westward tidal current reach maximum at about the same time (Fig. 9).

The total current is reduced or reversed when the tidal current and storm surge current contribute in opposite directions. An example is seen in Case I, at the second ebb tide 14 December, when the eastward storm surge current dominates the westward tidal current and prevents the reversal of the current (Fig. 8). The same situation occurred in Case II on the 22 December at the second ebb tide where the eastward storm surge current dominates the westward tidal current. Therefore, the total current continues in eastward direction during the ebb tide (Fig. 9). Figures 12 and 13 show respectively the tidal current and the total current

Fig. 9 Case II: 22–24 December 2004. Legend as in Fig. 8

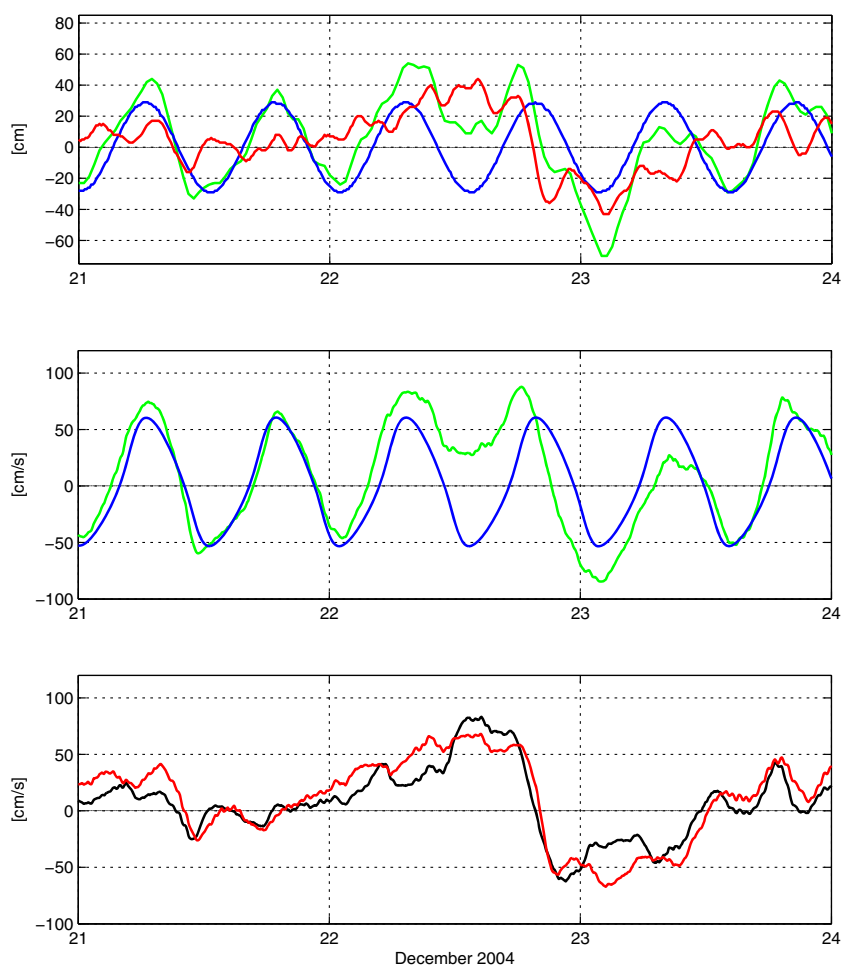
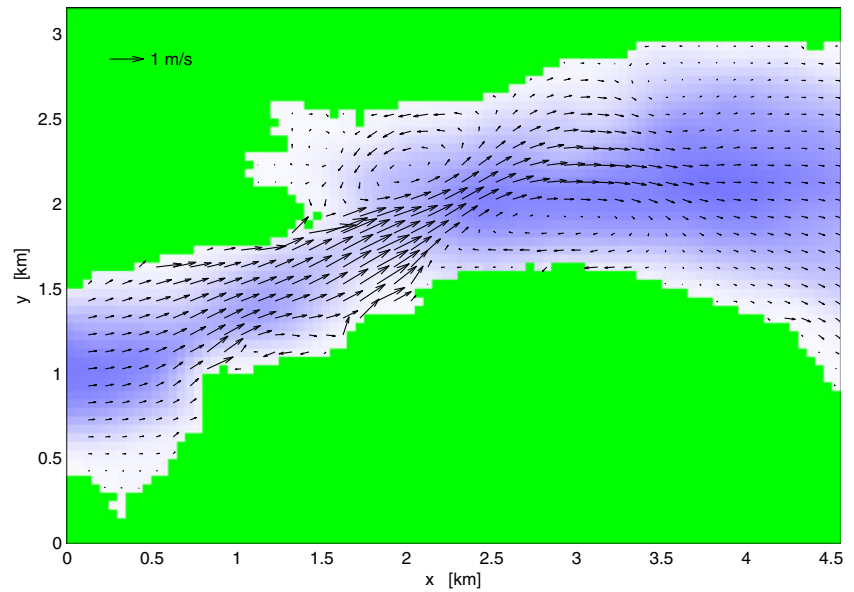


Fig. 10 Case I: The M_2 tidal current in Ballstad 15 December 2004 02:00 UT



at 13:00 UT 22 December in the Ballstadstraum, where the storm surge opposes the tidal current and reversing the direction of the total current and leading to a reduction of the speed.

In order to investigate how the current conditions changes when the storm surge occurs at other phases of the tidal cycle, we have modified Case II. The observed storm surge at Narvik and Harstad were artificially phase-shifted 5 h so that the maximum surge in Narvik coincides with the first high tide in Narvik 22 December 2004. The phase shifting enhances the interaction between the surge and the tide, and the total current through the cross section at the Ballstadstraum reaches about 10 cm s^{-1} higher than in Case II. This shows that maximum current speed can become larger than

in the two cases in December 2004 depending on in which phase of the tidal cycle the storm surge occurs.

5.2 Non-linear interaction

The non-linear interaction between the tidal current and the storm surge current can be studied by comparing the difference between the total current (simulated by M_2 + storm surge forcing at the open boundaries) and the tidal current, with the simulated storm surge current (lower panels, Figs. 8 and 9). When the tidal and the storm surge currents contribute in the same direction, the difference between the total current and the tidal current (black curve) is smaller than the storm surge current (red curve). Contrary,

Fig. 11 Case I: The total current (M_2 -tide+surge) in Ballstad 15 December 2004 02:00 UT

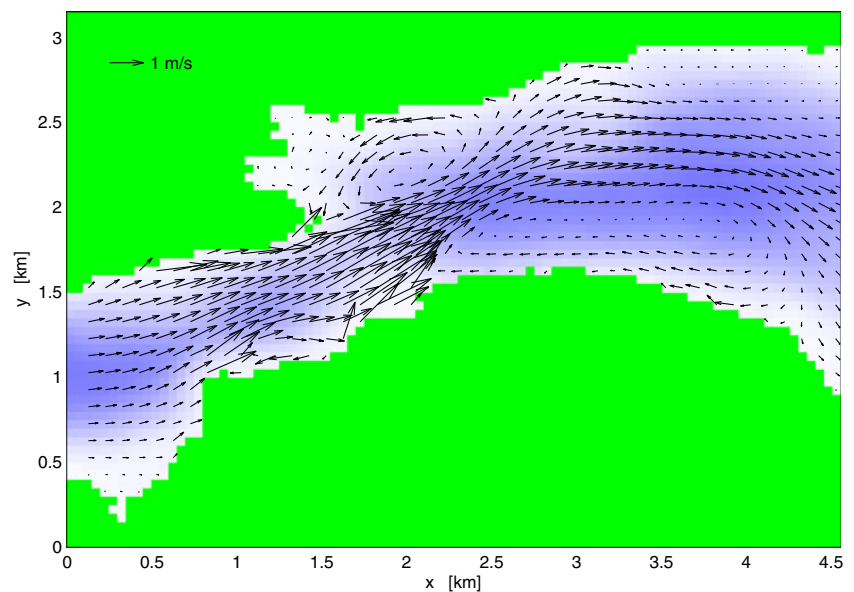
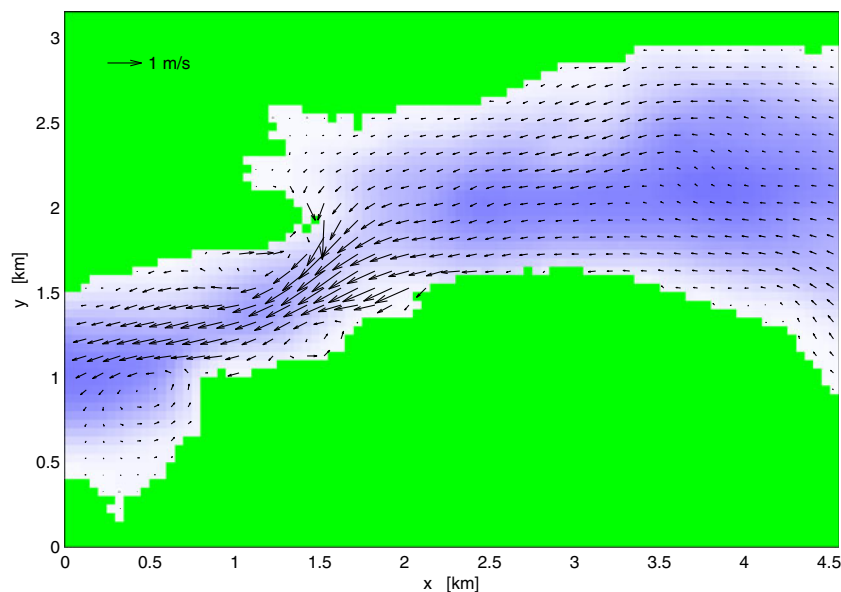


Fig. 12 Case II: The M_2 tidal current in Ballstad 22 December 2004 13:00 UT



the difference is larger when they contribute in opposite directions. This means that the storm surge current and the tidal current do not simply add, particularly when the tides and the storm surge contribute in the same direction and the total current is at its strongest. In this case, the effect of the interaction can reduce the effect of storm surge current with up to 50 % (i.e. Total current – tidal current \approx 50 % of storm surge current), see case I, 15 December (Fig. 8) and case II, 22 and 23 December (Fig. 9).

Studies of the dynamical interaction between tide and storm surge have earlier been carried out mainly for sea level elevation (Prandle and Wolf 1978; Tang et al. 1996). They demonstrated that the non-linear interaction mechanism is predominantly due to the quadratic bottom friction. To study

the dynamics of the mean current through a cross section in the Ballstadstraum (marked in Fig. 7), simulations with and without the non-linear advective terms in Eqs. 2 and 3 have been performed. The results from simulations without the non-linear advective terms show only small deviations from the simulations with non-linear advective terms. Similar results are found for other cross sections in the Tjeldsund channel. The major source of non-linear interaction as manifested in the *mean* total current through a cross section of the channel is hence mainly due to the non-linear bottom friction (4).

When the storm surge contributes to an intensified current, the bottom shear stress also increases and results in an increased bottom friction which acts on the current to slow

Fig. 13 Case II: The total current (M_2 -tide+surge) in Ballstad 22 December 2004 13:00 UT

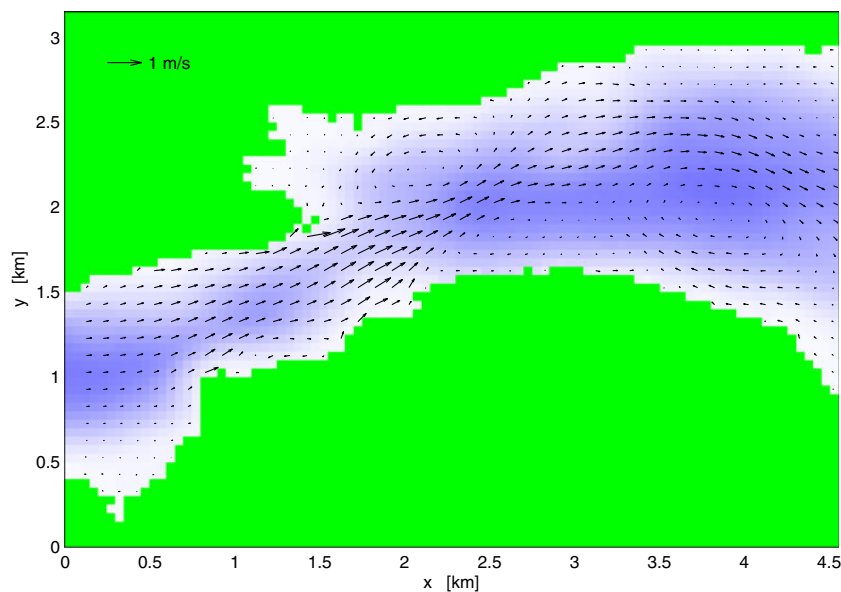
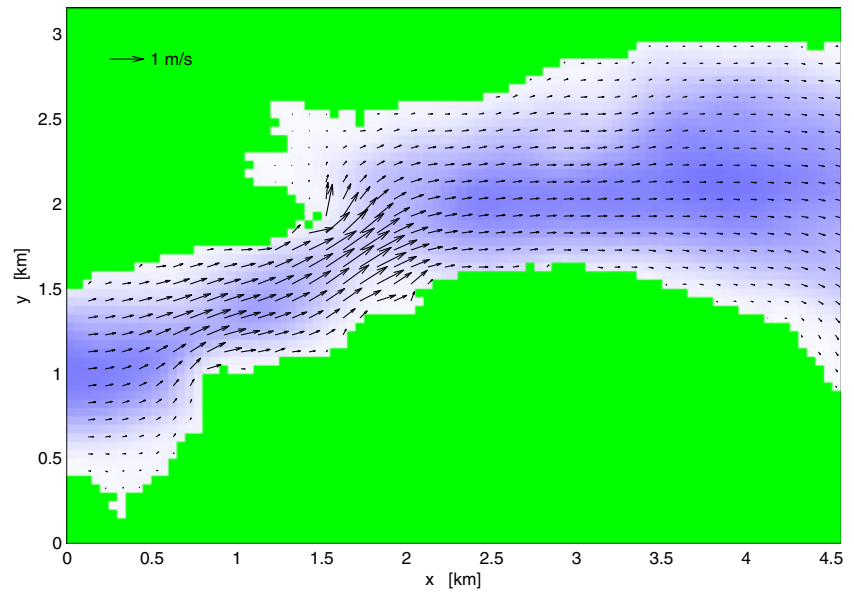


Fig. 14 Case I: The M_2 tidal current in Ballstad 15 December 2004 02:00 UT. Simulations without non-linear advective terms



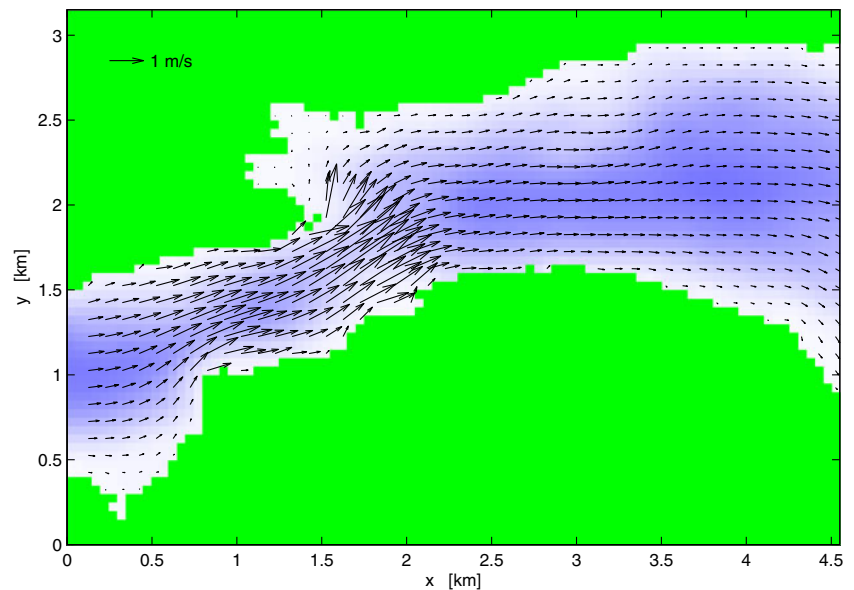
it down. This can explain that the difference between the total current and the tidal current (black curve) is smaller than the sole storm surge current (red curve) in the mean current through the cross section at the Ballstandstraum (lower panel, Figs. 8 and 9). When the storm surge and the tidal current contribute in opposite directions, the current is reduced or reversed resulting in a less energetic current, and hence also the effect of the bottom friction is reduced. In this case, the difference between the simulated total current and the simulated tidal current is larger than the simulated storm surge current due to the reduced effect of the bottom friction.

Although the non-linear advective terms have minor influence on the *mean* current through cross sections as

discussed above, these terms are essential for modelling of flow separation and shear flow instability. The two eddies seen in the Ballstadstraum in Figs. 10 and 11, one on the northern and the other (weaker) on the southern side, do not appear in simulations without the non-linear advective terms, see Figs. 14 and 15. It is interesting to discuss how the non-linear tide–surge interaction influence the strength of the eddies and formation of higher harmonics.

The formation of the two eddies which appear in the Ballstadstraum during eastward current in the simulations with non-linear advective terms (Figs. 10 and 11) is affected by the storm surge events. The eddy on the northern side is significantly enhanced in simulations when the tidal and storm surge currents both are in eastward direction (Fig. 11).

Fig. 15 Case I: The total current (M_2 -tide+surge) in Ballstad 15 December 2004 02:00 UT. Simulations without non-linear advective terms



The centre of the eddy on the southern side of the channel moves eastward with the eastward current. The extension of the eddy depends on the strength of the current and duration of the eastward current. Since the period of eastward current is prolonged by the storm surge (see Fig. 8), the eddy on the southern side is extended and the centre of the eddy moved eastward during the eastward storm surge current on December 15 (Fig. 11).

5.3 The modification of the tide due to non-linear interaction

In order to get more insight in how the tide–surge interaction modifies the tide at the time of the surge (see Jones and Davies 2008), we have used harmonic analysis to study the modification of the M_2 component and its main over-harmonics M_4 and M_6 . Time series of the modelled current at the six locations B1–B6 (marked in Fig. 7) have

been analysed by T-Tide (Pawlowicz et al. 2002) for time intervals of three and eight M_2 cycles. The time intervals have been chosen to cover the storm surge events. The analyses have been performed for simulations with boundary forcing from M_2 -tide only and the combined effect of M_2 -tide and storm surge, and for simulations both with and without the non-linear advective terms.

Tables 1 and 2 give the major and minor axis of the current ellipse and the orientation, Θ , of the major axis for M_2 and the corresponding over-harmonic M_4 and M_6 recognised in the tidal current and the total current (tide+surge). To cover the period of eastward storm surge current (see Fig. 8), a time interval of three M_2 cycles starting 13 December 2004 at 18:00 UT (Case I) is chosen for the analyses presented in Tables 1 and 2. The tables clearly show that the interaction between the tidal current and the storm surge current affects and changes M_2 and the corresponding over-harmonics. We see that especially the over-harmonic

Table 1 Major and minor axis for the M_2 current ellipse and the main higher harmonics for 6 locations in the Ballstadstraum (B1–B6) from the storm surge event December 2004

Location Depth	Constituent	Tide only			Total (Tide+Surge)		
		Major [cm s ⁻¹]	Minor [cm s ⁻¹]	Θ [deg]	Major [cm s ⁻¹]	Minor [cm s ⁻¹]	Θ [deg]
B1	M_2	92.4	-0.7	31.5	86.2	-1.8	34.9
6 m	M_4	5.0	-1.5	93.7	13.7	2.8	30.6
	M_6	10.1	0.6	27.7	2.6	-0.9	20.9
% of signal			99.8			83.3	
B2	M_2	78.3	-1.4	24.0	76.7	-2.1	25.3
22 m	M_4	8.2	-1.9	28.2	12.8	1.0	25.7
	M_6	9.8	1.1	20.9	2.7	-0.5	15.4
% of signal			99.6			83.9	
B3	M_2	15.8	0.5	33.7	22.7	1.9	31.6
8 m	M_4	10.9	2.0	28.9	8.9	1.4	28.1
	M_6	4.9	1.3	22.3	4.0	0.9	33.7
% of signal			97.1			61.5	
B4	M_2	15.5	-0.3	168.4	18.3	-1.3	165.6
12 m	M_4	3.3	-0.5	156.7	4.8	-1.2	170.7
	M_6	1.2	0.6	175.5	1.7	-0.2	169.7
% of signal			99.5			82.9	
B5	M_2	17.9	-0.4	166.2	16.4	-3.7	166.0
35 m	M_4	2.7	1.9	108.8	6.0	-1.0	178.3
	M_6	2.6	0.7	6.3	1.2	-0.5	39.1
% of signal			99.6			85.9	
B6	M_2	17.9	1.0	175.8	23.4	-2.9	165.4
47 m	M_4	1.6	-1.4	86.2	3.1	-0.4	111.6
	M_6	2.8	-1.1	97.6	1.7	0.2	128.7
% of signal			99.1			72.6	

The harmonic analyses are for a time interval of three M_2 cycles starting the 13 December at 18:00 UT. The orientation of the major axis (Θ) is relative east

Table 2 Major and minor axis for the M_2 current ellipse and the main higher harmonics for three locations in the Ballstadstraum (B1–B3) for simulations without the non-linear advective terms

Location Depth	Constituent	Tide only			Total (Tide+Surge)		
		Major [cm s ⁻¹]	Minor [cm s ⁻¹]	Θ [deg]	Major [cm s ⁻¹]	Minor [cm s ⁻¹]	Θ [deg]
B1	M_2	68.3	0.1	32.9	57.7	0.0	33.6
6 m	M_4	–	–	–	10.9	0.3	30.7
	M_6	5.1	0.2	24.8	1.6	0.0	37.3
% of signal			100.0			80.2	
B2	M_2	72.8	–0.2	24.6	61.7	–0.2	25.3
22 m	M_4	–	–	–	12.2	0.3	23.0
	M_6	6.8	0.3	21.1	1.8	0.1	27.5
% of signal			100.0			78.4	
B3	M_2	19.1	–0.6	21.8	16.9	–0.5	21.6
8 m	M_4	–	–	–	2.9	0.0	22.6
	M_6	1.4	0.0	23.6	0.3	0.0	14.8
% of signal			100.0			87.1	

The harmonic analyses are for a time interval of three M_2 cycles starting the 13 December at 18:00 UT. The orientation of the major axis (Θ) is relative east

components vary considerably from the tide only solution to the storm surge interacted solution. In addition, there is a spatial variation in how much the tidal constituents are modified due to the storm surge.

The error estimates from T-tide are quite small for the time series from simulations with tide only forcing, and larger for the time series from the total current, see Table 3.

For the locations in Table 1, only about 60–80 % of the total current from the combined tide and storm surge forcing is recognised as tidal signal. In interaction with the storm surge current, the major axis of the M_2 component was reduced in the total current at location B1 and B2, while an increase in the M_2 component was found at location B3 and B6 (see Table 1 for details). The results from the

harmonic analyses given in Table 1 show a spatial variation in interaction depending on the strength of the current and the depth at the location. There is a large difference in the modification of M_2 from B1 and B2 located in the narrowest and shallowest part of the channel to B3, within the eddy on the northern side of the Ballstadstraum, and B6 located in the deeper part of the channel. The quadratic bottom friction (4) depends on the magnitude of the current and the depth, and the results discussed above suggest that the variation of bottom friction across the channel is an important factor for the interaction mechanism and the modification of the M_2 component in the total current.

The simulations without the non-linear advective terms show a decrease in M_2 in the total current for the three locations B1, B2, and B3 presented in Table 2. In these simulations, the two large eddies located respectively north and south of the main current jet do not appear (see Figs. 14 and 15), and hence the current has an eastward direction for locations B1–B3.

The over-harmonic component M_4 increased in the total current for most of the locations. The increase was largest at shallow locations with strong current, e.g. location B1 (6 m depth) and B2 (22 m depth). At location B1, M_4 increased from 5.0 to 13.7 cm s⁻¹, see Table 1. There is also a considerable change in direction (Θ) of the major axis of M_4 of 57° at location B1. While there was an increase in M_4 for five of the six locations in Table 1, there was a small decrease in M_4 at the location B3 (8 m) located in the eddy on the northern side of the channel. At location B5 within the eddy

Table 3 Error estimates from T-tide from the harmonic analyses of the tidal current and the total current (tide+surge)

	Component	Tide only	Total (Tide+Surge)
Amplitude of			
major axis	M_2, M_4, M_6	0.1–0.3 cm s ⁻¹	0.6–1.8 cm s ⁻¹
Orientation of			
major axis	M_2	0.1–0.6°	0.9–3.6°
	M_4	0.6–4.5° ^a (17.5° at B6)	5.3–8.9° ^a (13.2° at B6)
	M_6	0.9–3.6°	11.9–33.7° ^a (69.1° at B5)

^afor most locations

at the southern side of the channel, there was an increase in M_4 and also a change in the orientation of the M_4 major axis of 69.5° (error estimate of 8.9°) which can be associated with the eastward motion and expansion of the eddy during the storm surge as discussed above. As found for the tidal M_2 constituent, a spatial variation of the effect of the tide–surge interaction was also found for the M_4 constituent. Spatial variations in the over-harmonics due to tide–surge interaction are also reported by Jones and Davies (2008).

The over-harmonic M_4 is not present in the simulations with tide only forcing without non-linear advective terms, but increases to about 10 cm s^{-1} in the most energetic part of the current (i.e. locations B1 and B2) in simulations with tide+surge forcing (Table 2). The absence of the M_4 component in the simulation with tide only forcing and without the non-linear advective terms confirms that the M_4 component is generated from the M_2 tide by non-linear interaction and

that the non-linear advective terms are essential, as pointed out by Jones and Davies (2008). Since M_4 is generated in simulations without the non-linear advective terms, but with tide + surge forcing, there is some energy in the M_4 frequency band in the storm surge signal. Harmonic analysis of the estimated surge used as boundary input shows that indeed the surge signal contains some energy in the near M_4 band. Therefore, the calculated M_4 amplitude is not only an effect of non-linear interaction.

A transient storm surge forcing which contains energy on periods corresponding to the tidal over-harmonics will lead to corresponding periods in the current field. In order to quantify this effect, we have examined an idealized steady state storm surge forcing in a similar way as done by Jones and Davies (2008). A constant sea level elevation of 50 cm was applied at the southern boundary of the Tjeldsund channel in addition to the M_2 tide for the same period

Table 4 Major and minor axis for the M_2 current ellipse and the main higher harmonics for 6 locations in the Ballstadstraum (B1–B6) from the steady state storm surge

Location Depth	Constituent	Tide only			Total (Tide+Surge)		
		Major [cm s ⁻¹]	Minor [cm s ⁻¹]	Θ [deg]	Major [cm s ⁻¹]	Minor [cm s ⁻¹]	Θ [deg]
B1	M_2	92.4	−0.7	31.5	57.5	−0.9	38.3
6 m	M_4	5.0	−1.5	93.7	2.1	−0.1	26.0
	M_6	10.1	0.6	27.7	0.1	0.0	60.5
	% of signal		99.8			100.0	
B2	M_2	78.3	−1.4	24.0	51.1	−1.1	27.1
22 m	M_4	8.2	−1.9	28.2	1.5	−0.1	37.2
	M_6	9.8	1.1	20.9	0.3	−0.0	33.9
	% of signal		99.6			100.0	
B3	M_2	15.8	0.5	33.7	22.9	1.6	29.4
8 m	M_4	10.9	2.0	28.9	1.4	0.2	32.9
	M_6	4.9	1.3	22.3	0.4	0.1	31.4
	% of signal		97.1			100.0	
B4	M_2	15.5	−0.3	168.4	14.8	−2.7	169.5
12 m	M_4	3.3	−0.5	156.7	4.8	−1.3	177.1
	M_6	1.2	0.6	175.5	2.3	−0.6	178.5
	% of signal		99.7			99.6	
B5	M_2	17.9	−0.4	166.2	10.1	−3.8	163.1
35 m	M_4	2.7	1.9	108.8	2.5	−1.6	5.4
	M_6	2.6	0.7	6.3	0.9	−0.5	57.1
	% of signal		99.6			99.9	
B6	M_2	17.9	1.0	175.8	23.3	−1.5	163.0
47 m	M_4	1.6	−1.4	86.2	3.3	1.1	131.5
	M_6	2.8	−1.1	97.6	1.1	0.8	67.5
	% of signal		99.1			100.0	

The harmonic analyses are for a time interval of three M_2 cycles starting the 13 December at 18:00 UT. The orientation of the major axis (Θ) is relative east

as the storm surge event in December 2004. Non-linear simulations with this steady state surge shows that the over-harmonic component M_4 decreases at five of the locations (B1–B6, Table 4) as compared with the results for the transient eastward storm surge (Table 1). This confirms that the transient eastward storm surge current contain energy in the near M_4 band and that harmonic constituent M_4 is affected by this in the tide–surge interaction.

The M_6 component decreases at all locations except B4 by the tide–surge interaction in the transient storm surge, at the latter, there is a small increase (Table 1). At B1, M_6 is reduced with 7.5 cm s^{-1} from the tidal only to the total current, and a reduction of 7.1 cm s^{-1} was found at B2. A diurnal K_1 component was also recognised in both the storm surge current and the total current, an effect of the diurnal variation of the storm surge.

The harmonic analyses were also performed for a period of eight M_2 cycles with start time 13 December 2004 at 00:00 (UT), i.e. 18 h earlier than the analyses performed for a period of three M_2 cycles. The analyses of time series with a period of eight M_2 cycles gives some different results in modification of the tidal current components by the tide–surge interaction than the analyses performed for a period of three M_2 cycles. For example, the M_2 component at location B3 is clearly less increased when the analyses are performed for a period of eight M_2 cycles. The results in this section are presented to cover the eastward storm surge current with a period of about three M_2 cycles introduced in the beginning of the storm surge event, i.e. the results from harmonic analyses of the relative short time series with a period of three M_2 cycles. Since the period of the eastward storm surge

current is shorter than eight M_2 cycles, the impact of the tide–surge interaction would be smaller in analyses of time series with a period of eight M_2 cycles.

6 Comparison with field measurements

From November 2004 to March 2005, current measurements were executed with acoustic current meters (Aquadopp, from Nortek AS) by The Norwegian Defence Research Establishment at two locations, the Steinslandsstraum and the Ballstadstraum. The two stations are marked by St1 and St2 in Fig. 2, respectively. Measurements were made at two levels, 23 and 40 m below surface at the Steinslandstraum and 22 and 30 m below surface at the Ballstadstraum. In periods with strong currents, the pressure records, especially from the Ballstadstraum, indicate that the upper part of the rig has been bent down. The current data show a considerable amount of high-frequency current oscillations both in strength and direction (station St2 is shown in Figs. 16 and 17). The periods of these oscillations are about 1 h and shorter, and cannot be related to any over-harmonic tidal oscillations. These short periodic oscillations represent a considerable amount of energy and partly contaminate the tidal oscillations. Whether these oscillations are physical or artificial due to the deflection of the rig has not been possible to determine. Earlier current measurements at station SK do not show the same amount of high-frequency oscillations and the observed tidal current from station SK agrees much better with model predictions (see Section 3).

Fig. 16 Case I: Comparison between modelled (green) and observed (red) current at station St2, in Ballstadstraumen. Upper panel: Current speed. Lower panel: Current direction relative north (degree True)

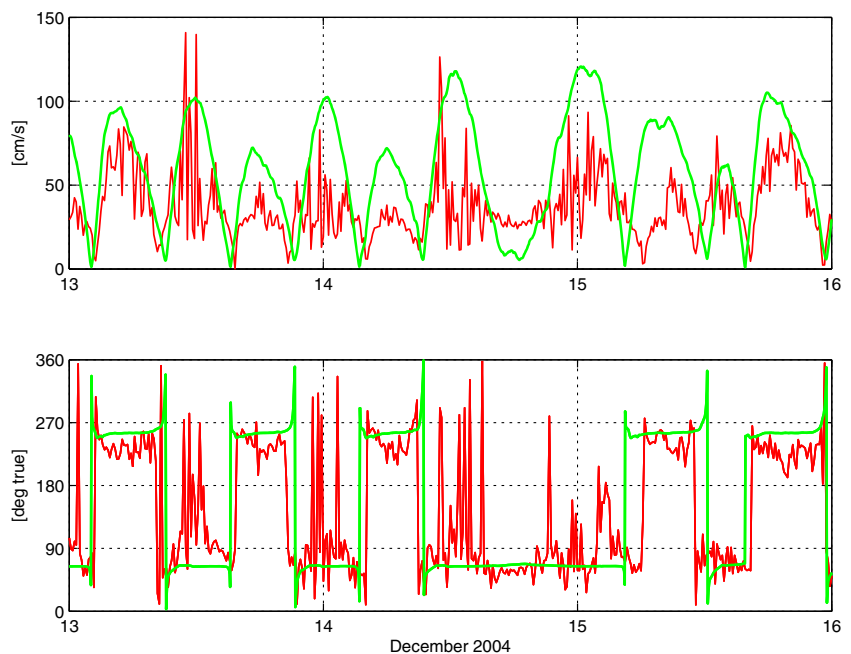
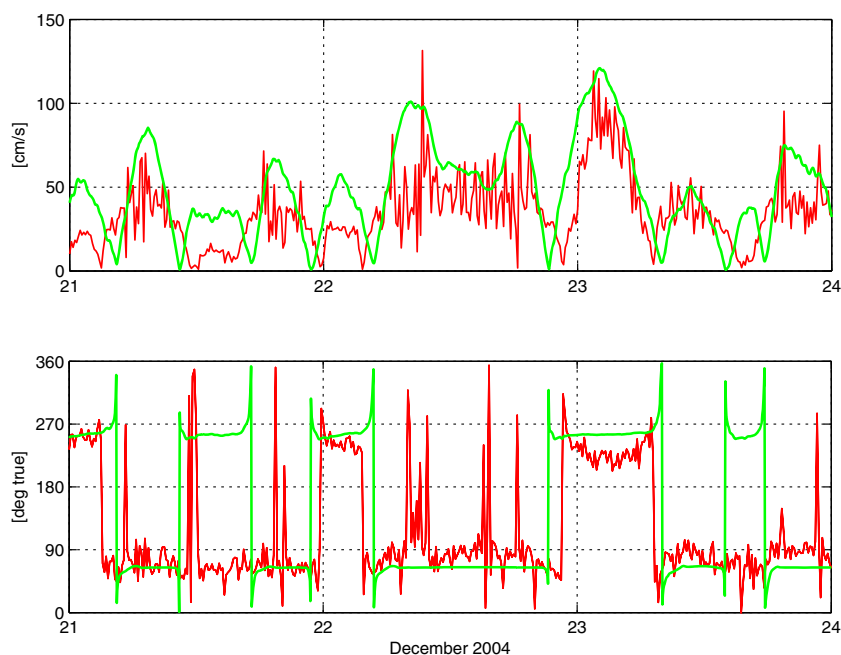


Fig. 17 Case II : Comparison between modelled (*green*) and observed (*red*) current at station St2, in Ballstadstraumen 21–23 December 2004. *Upper panel:* Current speed. *Lower panel:* Current direction relative north (degree True)



Model simulations with observed sea level imposed at the open boundaries, extrapolated as described in Section 2.2, have been performed for the period of the storm surge events (case I and case II) in order to compare model simulations with the current measurements. Figures 16 and 17 show the simulated current and the observed current at station St2 in the Ballstadstraum. Generally, the model is able to reproduce the main features of the current variation, but the model over-predicts the current strength. For Case I (Fig. 16), the model predicts well the eastward current where the storm surge current dominates the tidal current on 14 December and prevent the reversal of the current. Similarly in case II on 22 December (Fig. 17). For Case II on 23 December, the model also shows that the period with westward current is prolonged compared to the tidal period in agreement with observations. The model does not show the high-frequency oscillations which are dominant in the observations, but these oscillations may be due to mooring oscillations as discussed above.

7 Concluding remarks

This study demonstrates clearly the complex flow features of the tidal- and the storm surge-driven currents in a narrow channel connecting two separate fjord systems. Two storm surge events from December 2004 have been studied in details.

During the storm surge events, the large-scale external surge introduced an additional sea level difference between the northern and southern entrance of the Tjeldsund channel. This lead to a storm surge current that was found to

intensify or reduce the tidal current and also reverse the direction of the current. The non-linear interaction between the tide and the surge is evident in the mean tidal current and the mean storm surge current through a cross section of the channel. For the mean current through the channel, the non-linear bottom friction is found to be the main source of the tide–surge interaction. This is in accordance with the results by Prandle and Wolf (1978) and Tang et al. (1996).

Although the non-linear advective terms have minor influence on the interaction displayed by the mean current, they influence the eddy formation and flow separation, and therefore locally have a strong effect on the over-harmonic current components, as also demonstrated by Jones and Davies (2008). They discuss the modification of M_2 , M_4 , and M_6 by the tide–surge interaction with different wind forcings in a very shallow area in the eastern Irish Sea. They found that there are significant non-linear effects which influence both the computed tidal elevation and tidal current distribution. In our experiments, the non-linear advective terms are found to be important for the formation of eddies. The eddies that appear in simulations with the non-linear advective terms do not appear in simulations without these terms. The non-linear advective terms are also found to be important for the generation of the over-harmonic M_4 constituent. This was demonstrated by comparing the tide only forced current with and without the non-linear advective terms where the M_4 constituent is not present in tidal simulations without the non-linear advective terms.

Time series of the tide only forced current and the total current, forced by tide+surge at the open boundaries, from

six locations in the Ballstadstraum have been harmonic analysed and compared. The analyses show that the tidal constituent M_2 and the corresponding over-harmonics are clearly modified during the storm surge by the interaction between the tidal current and the storm surge current. Especially the results from the harmonic analyses suggest that the non-linear bottom friction is an important factor for the modification of the tidal M_2 component.

The study clearly shows that in a narrow and shallow channel like the Tjeldsund channel, tide–surge interaction will occur during storm surge events. The modification of the constituent M_2 and its over-harmonics shows that tide–surge interaction leads to modification of the tide. Consequently, a “classical” de-tiding procedure will result in tidal energy being left in the surge signal as pointed out by Jones and Davies (2008). Hence when modelling the current during a storm surge event, it will be necessary to model the total current during the storm surge.

In this study, we have forced the storm surge current in the channel system by the observed sea level difference between the ends of the channel and neglected the local wind stress and atmospheric pressure differences. Comparison with observations indicates that this approach is justified and may be useful for future modelling in similar cases.

Acknowledgments The work with this paper has been supported by The Norwegian Hydrographic Service. The modelling work has been supported by The Norwegian Defence Research Establishment (FFI), Kjeller under a grant FFI-0352. FFI has in cooperation with NHS, Stavanger, executed a field campaign for recoding current data. NHS provided depth matrix and sea level data both from permanent and temporary stations within the area.

References

- Bobanovic J, Thompson KR, Desjardins S, Ritchie H (2006) Forecasting storm surges along the east coast of Canada and the north-eastern United States: the storm of 21 January 2000. *Atmos.-Ocean* 44(2):151–161
- Davies AM, Jones JE, Xing J (1997a) Review of recent developments in tidal hydrodynamic modeling. 1: spectral models. *J Hydraul Eng* 123(4):278–292
- Davies AM, Jones JE, Xing J (1997b) Review of recent developments in tidal hydrodynamic modeling. 2: turbulence energy models. *J Hydraul Eng* 123(4):293–302
- Gjevik B, Moe H, Ommundsen A (1997) Sources of the maelstrom. *Nature* 388(6645):837–838
- Gjevik B, Hareide D, Lyngre BK, Ommundsen A, Skailand J, Urheim H (2006) Implementation of high resolution tidal current fields in electronic charts systems. *J Mar Geodesy* 29(1):1–17
- Hjelmervik KB, Trulsen K (2009) Freak wave statistics on collinear currents. *J Fluid Mech* 637:267–284
- Hjelmervik K, Ommundsen A, Gjevik B (2005) Implementation of non-linear advection terms in a high resolution tidal model. Technical report, Preprint Series No. 1, Dept. Math. University of Oslo, Norway, ISSN 0809–4403
- Hjelmervik K, Lyngre B, Ommundsen A, Gjevik B (2009) Modelling of tides and storm surges in the Tjeldsund channel in northern Norway. In: PhD Thesis Hjelmervik: Wave–current interactions in coastal tidal currents. Faculty of Mathematics and Natural Sciences, University of Oslo
- Horsburgh KJ, Wilson C (2007) Tide-surge interaction and its role in the distribution of surge residuals in the North Sea. *J Geophys Res* 112. doi:10.1029/2006JC004033
- Johns B, Rao AD, Dube SK, Sinha PC (1985) Numerical modeling of tide–surge interaction in the Bay of Bengal. *Philos Trans Roy Soc Lond A* 313(1526):507–535
- Jones JE, Davies AM (2007) Influence of non-linear effects upon surge elevations along the west coast of Britain. *Ocean Dyn* 57(4–5):401–416
- Jones JE, Davies AM (2008) On the modification of tides in shallow water regions by wind effects. *J Geophys Res Oceans* 113(C5):C05014. doi:10.1029/2007JC004310
- Martinsen EA, Engedahl H (1987) Implementation and testing of a lateral boundary scheme as an open boundary-condition in a barotropic ocean model. *Coast Eng* 11(5–6):603–627
- Mesinger F, Arakawa A (1976) Numerical methods used in atmospheric models. Garp Publication Series No 17, WMO-ICSU
- Moe H, Ommundsen A, Gjevik B (2002) A high resolution tidal model for the area around The Lofoten Islands, northern Norway. *Cont Shelf Res* 22(3):485–504
- Pawlowicz R, Beardsley B, Lentz S (2002) Classical tidal harmonic analysis including error estimates in Matlab using T-TIDE. *Comput Geosci* 28(8):929–937
- Prandle D, Wolf J (1978) The interaction of surge and tide in North sea and River Thames. *Geophys J R Astron Soc* 55(1):203–216
- Smagorinsky J (1963) General circulation experiments with the primitive equations. *Mon Weather Rev* 91(3):99–164
- Sutherland G, Garrett C, Foreman M (2005) Tidal resonance in Juan de Fuca Strait and the Strait of Georgia. *J Phys Oceanogr* 35(7):1279–1286
- Tang YM, Grimshaw R, Sanderson B, Holland G (1996) A numerical study of storm surges and tides, with application to the North Queensland coast. *J Phys Oceanogr* 26(12):2700–2711